



## OPEN ACCESS

## EDITED BY

Lijie Guo,  
Beijing Mining and Metallurgy  
Technology Group Co., Ltd., China

## REVIEWED BY

Shuhua Liu,  
Wuhan University, China  
Zengqi Zhang,  
University of Science and Technology  
Beijing, China

## \*CORRESPONDENCE

Changlong Wang,  
✉ baistuwong@139.com  
Yongxiang Zhou,  
✉ zhouyx@bjut.edu.cn

RECEIVED 08 March 2023

ACCEPTED 03 April 2023

PUBLISHED 18 April 2023

## CITATION

Zhang H, Qi Y, Jing J, Wang C, Zhou Y,  
Zhang K, Zheng Y, Zhai Y and Liu F (2023),  
Properties and environmental impact of  
building foundation pit backfilling  
materials containing iron and steel  
solid waste.  
*Front. Earth Sci.* 11:1181974.  
doi: 10.3389/feart.2023.1181974

## COPYRIGHT

© 2023 Zhang, Qi, Jing, Wang, Zhou,  
Zhang, Zheng, Zhai and Liu. This is an  
open-access article distributed under the  
terms of the [Creative Commons  
Attribution License \(CC BY\)](https://creativecommons.org/licenses/by/4.0/). The use,  
distribution or reproduction in other  
forums is permitted, provided the original  
author(s) and the copyright owner(s) are  
credited and that the original publication  
in this journal is cited, in accordance with  
accepted academic practice. No use,  
distribution or reproduction is permitted  
which does not comply with these terms.

# Properties and environmental impact of building foundation pit backfilling materials containing iron and steel solid waste

Hongze Zhang<sup>1</sup>, Yang Qi<sup>2</sup>, Jianlin Jing<sup>2</sup>, Changlong Wang<sup>2\*</sup>,  
Yongxiang Zhou<sup>3\*</sup>, Kaifan Zhang<sup>2</sup>, Yongchao Zheng<sup>4</sup>, Yuxin Zhai<sup>5</sup>  
and Feng Liu<sup>6</sup>

<sup>1</sup>School of Earth Science and Surveying and Mapping, China University of Mining and Technology (Beijing), Beijing, China, <sup>2</sup>Collaborative Innovation Center for Intelligent Regulation and Integrated Management of Water Resources Jointly Built by Provinces and Ministries, School of Civil Engineering, Hebei University of Engineering, Handan, China, <sup>3</sup>Faculty of Architecture, Civil and Transportation Engineering, Beijing University of Technology, Beijing, China, <sup>4</sup>State Key Laboratory of Solid Waste Reuse for Building Materials, Beijing Building Materials Academy of Science Research, Beijing, China, <sup>5</sup>Technical Center, China Railway Construction Group Co., Ltd., Beijing, China, <sup>6</sup>Construction Development Co., Ltd., China Railway Construction Group, Baoding, China

**Introduction:** In order to promote the comprehensive utilization of iron and steel solid waste, steel slag (SS), granulated blast furnace slag (GBFS), and flue gas desulfurization gypsum (FGDG) were used as raw materials to replace cement to prepare the full solid waste premixed solidified agent (PSA). Then PSA, iron ore tailings (IOTs), and water were mixed to prepare building foundation pit backfilling materials (BFPBM).

**Methods:** Various tests were conducted to investigate the effects of SS fineness, SS content and mixing ratio of PSA on the properties of PFPBM, including mechanical property test, X-ray diffraction (XRD), scanning electronic microscopy (SEM), energy dispersive spectrometry (EDS) and synthetic precipitation leaching procedure (SPLP). The stability of the BFPBM was tested and the hydration mechanism of the PSA was analyzed.

**Results:** The results show that when the specific surface area (SSA) of SS is 457 m<sup>2</sup>·kg<sup>-1</sup>, the paste mass concentration (PMC) is 79%, the mixing ratio of PSA is 20%, and the mix proportion of PSA is SS: FGDG: GBFS = 58:10:32. In this case, water-reducing agent (WRA) accounting for 0.18% of the total amount of PSA is added. The 28d compressive strength of BFPBM is greater than 0.40 MPa with the maximum value of 6.22 MPa, and the mixture slump of BFPBM is greater than 215 mm, which meets the index requirements of Chinese National Standard T/CECS 1037-2022 *Technical Standard for Backfilling Project by Using Premixed Fluidized Solidified Soil*.

**Discussion:** According to the mechanism study, the mineral phases of the PSA after hydration are: C<sub>2</sub>S, C<sub>3</sub>S, Ca (OH)<sub>2</sub>, ettringite (AFT), C-S-H gel, and RO phase. C<sub>2</sub>S, C<sub>3</sub>S, CaSO<sub>4</sub> and other substances gradually disappeared with the hydration, while the content of AFT and C-S-H gel substances increased. BFPBM prepared from iron and steel waste has high strength and environmental friendliness, making it have good application prospects in foundation pit backfilling and mine filling.

## KEYWORDS

iron and steel solid waste, steel slag (SS), granulated blast furnace slag (GBFS), premixed solidified agent (PSA), building foundation pit backfilling materials (BFPBM), mixture slump, ettringite (AFT)

## 1 Introduction

With the acceleration of urban construction, building foundation pit backfilling materials (BFPBM) prepared via premixed solidified agent (PSA) which mainly contains cement or lime are widely used in filling projects (Ning and Huang, 2006; Abdi et al., 2021; Sun et al., 2021). In China, cement production is a traditional industry with high emissions and energy consumption. The annual CO<sub>2</sub> emissions account for 5%–8% of global emissions (Turner and Collins, 2013; Mo et al., 2017). Therefore, to achieve low-carbon and high-quality development, it is urgent to develop new materials to replace cement-based PSA in the current infrastructure industry. Although China has a huge stock of industrial solid waste, such as coal gangue, red mud, tailings, smelting slag, phosphogypsum, electrolytic manganese slag, fly ash, coal gasification slag, and so on. But the comprehensive utilization rate is only 62.3%, lower than that of western countries.

Steel slag (SS) is the main metallurgical slag of the Chinese iron and steel industry. The SS emission is roughly 12–20% of crude steel output (Shi, 2004; Guo et al., 2018; Dhoble and Ahmed, 2018). In China, the annual production of SS is about 80 million tons, and the cumulative storage is around 800 million tons (Zhuang and Wang, 2021; Zhang et al., 2022; Zhao et al., 2022). However, less than 30% of SS has been utilized comprehensively (Alanyali et al., 2009; Li et al., 2011; Wang et al., 2018). In terms of chemical composition, SS mainly consists of CaO, SiO<sub>2</sub>, Fe<sub>2</sub>O<sub>3</sub>, and MgO, plus a small amount of Al<sub>2</sub>O<sub>3</sub>, P<sub>2</sub>O<sub>5</sub>, and MnO (Roslan et al., 2016; Peng and Huang, 2010; Shi, 2002). The main minerals in SS include C<sub>2</sub>S (2CaO·SiO<sub>2</sub>), C<sub>3</sub>S (3CaO·SiO<sub>2</sub>), C<sub>2</sub>F (2CaO·Fe<sub>2</sub>O<sub>3</sub>), RO phase (a continuous solid solution composed of divalent metal oxides like FeO, MgO, MnO, and CaO), Fe, and free CaO (f-CaO) (Yan et al., 2014; Yüksel, 2017; Humbert and Castro-Gomes, 2019; Liu et al., 2020; Liu et al., 2020; Gencel et al., 2021). Overall, SS has similar chemical and mineral compositions as cement. At present, SS is mainly used in subgrade engineering (Gu et al., 2018; Aldeeky and Hattamleh, 2017; Wang et al., 2020), mine filling (Li et al., 2021; Zhang et al., 2020; Zhao et al., 2022), and asphalt concrete aggregate production (Hasita et al., 2020; Hasita et al., 2020; Jiao et al., 2020). The C<sub>2</sub>S and C<sub>3</sub>S in SS can react with water to generate many hydration products, such as C-S-H gel (3CaO·2SiO<sub>2</sub>·3H<sub>2</sub>O), C-A-H crystal (CaO·Al<sub>2</sub>O<sub>3</sub>·10H<sub>2</sub>O), Ca(OH)<sub>2</sub>, and C-A-S-H gel (CaO·Al<sub>2</sub>O<sub>3</sub>·4SiO<sub>2</sub>·5H<sub>2</sub>O). SS provides a promising auxiliary cementitious material, which could reduce resource waste and protect the environment (Palankar et al., 2016; Zhao et al., 2016; Zhuang and Wang, 2021). Thus, replacing cement and lime with metallurgical wastes is feasible to prepare new curing agents (Huang et al., 2020; Wang et al., 2021).

In recent years, scholars at home and abroad have carried out research on the preparation of BFPBM with PSA of steel waste. Yu et al. (2021) concluded that clay minerals have a great effect on soil engineering characteristics when using carbonized SS to prepare PSA and stabilize soil filling. Shen et al. (2018) used flue gas desulfurization gypsum (FGDG), SS, and clinker-free cement to prepare PSA to solidify the soft soil. When the mixing ratio of PSA is 5% higher than that of P·O 42.5R, the curing effect is similar. Deng et al. (2018) solidified the soft soil with PSA containing 20% SS, and the 28d compressive strength of the solidified soft soil could reach 1.2 MPa; Wang and Wang (2022) used industrial waste slags such as granulated blast furnace slag (GBFS) and calcium carbide slag to

solidify soil with cement. It was found that the production of erosion products was related to the CaO content of waste slag. Sun et al. (2021) concluded that with the dosage of 10% PSA, the 7d unconfined compressive strength of the prepared material was 3.46 MPa, meeting the requirements of all levels of highway pavement base with light traffic load. However, in the preparation of PSA from metallurgical slag, cement and metallurgical slag are used as raw materials, and the dosage of metallurgical slag is generally low. In the existing studies on PSA mixed with SS, most focus on accelerating the hydration process of SS and activating cementitious activity, while only a few studies are conducted to synergistically activate the physical and chemical activation of SS. The SS activated by mechanical force and mixed with GBFS and FGDG can ensure the soundness of the cementitious system and promote the generation of hydration products in the later stage. Adding and dissolving FGDG can provide conditions for the formation of ettringite (Xu et al., 2019; You et al., 2020; Zhang et al., 2020; Zhuang and Wang, 2021).

In this paper, steel waste (SS, GBFS, iron ore tailings (IOTs), FGDG) was used as raw materials to prepare full solid waste PSA and BFPBM to completely replace cement. Besides, the influences of SS fineness and content, and the mixing ratio of PSA on the performance of BFPBM were studied through various tests, including mechanical property test, X-ray diffraction (XRD), and energy dispersive spectrometry (EDS). In addition, the PSA stability and hydration mechanism were tested. Finally, synthetic precipitation leaching procedure (SPLP) was adopted to test the leaching of heavy metals from the solidified body. This paper provides theoretical and technical support for the application of iron and steel metallurgical wastes in construction and mine engineering.

## 2 Materials and methods

### 2.1 Experimental materials

- SS. The SS used is the converter steel slag with the content of f-CaO as 2.85% and of f-MgO as 2.29%. The active coefficient and alkalinity value can reflect the activity of SS to a certain extent. The active coefficient is the ratio of active ingredients to inert ingredients, HAI=0.38. The alkalinity value is calculated through the Mason's method (Mason, 1944). According to the alkalinity value, SS can be classified as low-alkalinity SS (<1.8), medium-alkalinity SS (1.8–2.5), and high-alkalinity SS (>2.5). The alkalinity value of the used SS is 3.175, indicating that it has high-alkalinity. The particle size distribution analysis shows that 86.12% of the SS particles have the diameter between 0.3mm and 9.5 mm. Thus, the SS should be broken before grinding. The chemical composition of SS is listed in Table 1 and the major chemical components are CaO, Fe<sub>2</sub>O<sub>3</sub> and SiO<sub>2</sub>. Mineral phases of SS are C<sub>3</sub>S, C<sub>2</sub>S, and RO phases (FeO, MnO, and solid solution of MgO) (See Figure 1A).
- IOTs. The density of IOTs used in the test is 3.20 g cm<sup>-3</sup>. The major components are inorganic constituents, such as SiO<sub>2</sub>, CaO, MgO, Fe<sub>2</sub>O<sub>3</sub>, and Al<sub>2</sub>O<sub>3</sub>. As the content of SiO<sub>2</sub> in IOTs is 73.15% (>60%), the IOTs belong to high silica mineral materials. As can be seen from Figure 2, most of the IOTs particles are between 0.3 and 1.18 mm in size, accounting for 64.43%.

TABLE 1 Chemical composition of raw materials (mass fraction, %).

Materials	CaO	SiO <sub>2</sub>	Fe <sub>2</sub> O <sub>3</sub>	MgO	Al <sub>2</sub> O <sub>3</sub>	TiO <sub>2</sub>	Na <sub>2</sub> O	K <sub>2</sub> O	SO <sub>3</sub>	Others
SS	33.56	9.10	27.31	7.96	4.32	0.12	0.11	0.06	0.36	10.91
GBFS	38.14	29.94	0.48	9.82	16.90	1.35	0.23	0.38	1.66	1.10
FGDG	37.98	0.56	0.45	0.08	1.13	0.02	0.03	0.06	51.27	8.55
IOTs	3.19	73.15	7.41	3.42	6.28	0.09	0.65	2.05	0.59	2.01

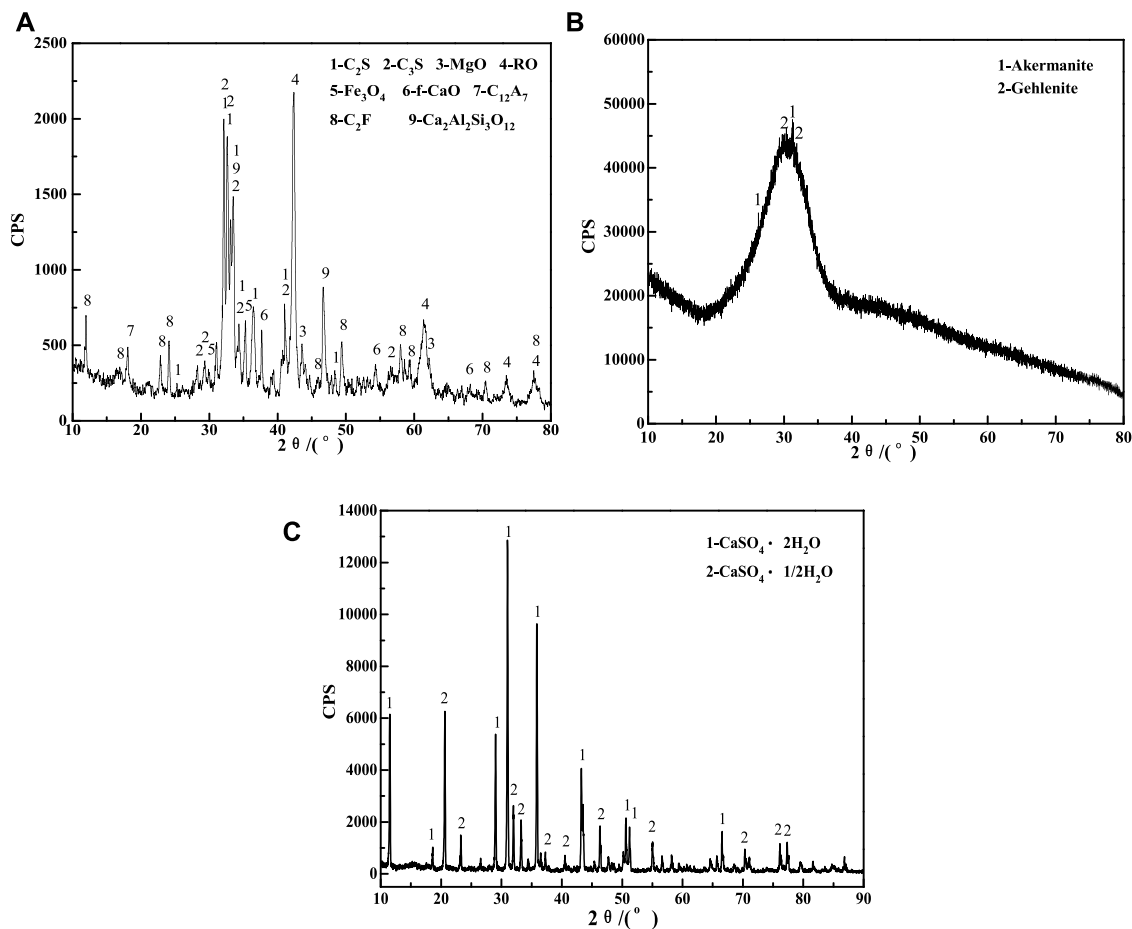
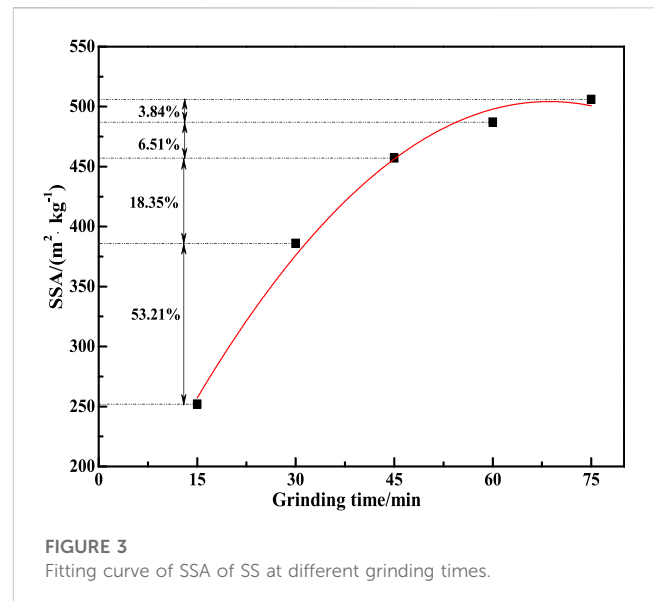
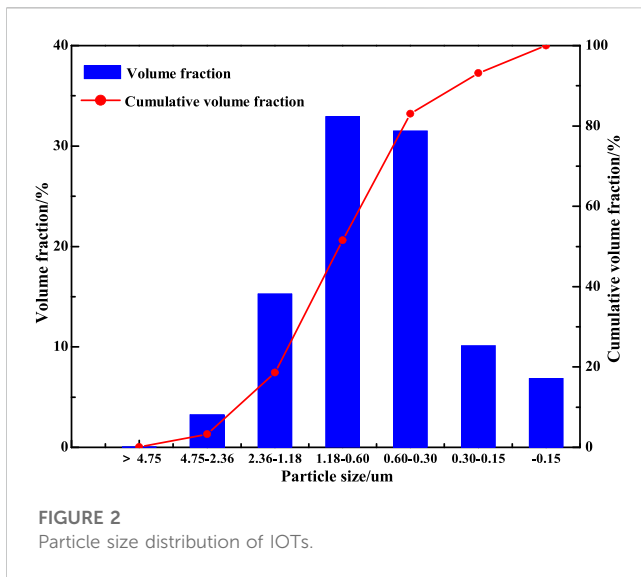


FIGURE 1 XRD patterns of raw materials. (A) SS; (B) GBFS; (C) FGDG.

- (3) GBFS. The particle size of GBFS is 0.2–6 mm, and the apparent density is  $2.86 \times 10^3 \text{ kg} \cdot \text{m}^{-3}$ . According to the chemical composition of the used GBFS, the alkalinity value is 1.024 and it belongs to alkaline GBFS. The quality coefficient K is 2.058 ( $>1.2$ ) and the larger the K value, the better. The active coefficient  $M_a$  is 0.564 ( $>0.3$ ), indicating that it belongs to highly-active GBFS. Figure 1B shows the XRD patterns. It can be seen that there is an obvious peak at 25–35°, which is indicating that GBFS belongs to vitreous substance.
- (4) FGDG. The chemical composition of FGDG is listed in Table 1. The major components are  $\text{CaSO}_4 \cdot 2\text{H}_2\text{O}$  and  $\text{CaSO}_4 \cdot 1/2\text{H}_2\text{O}$  (Figure 1C).
- (5) Other materials. In the test, the water-reducing agent (WRA) is polycarboxylates high performance water-reducing admixture (PC) whose water-reducing rate is 25%. P-O 42.5 ordinary Portland cement (OPC) is used in the contrast test.

## 2.2 Experimental method

- (1) PSA preparation. Firstly, SS (ground into 1–3 mm particles with a jaw crusher), GBFS, and FGDG were put in the oven at 105°C for 24 h. Then, they were milled separately with the SMΦ 500 mm × 500 mm laboratory ball mill. Finally, the



pulverized raw materials were mixed according to the optimal ratio, thus obtaining the PSA.

- (2) Preparation and testing of paste samples. The water requirement of normal consistency of PSA was determined according to GB/T 1346–2011 *Test methods for water requirement of normal consistency, setting time and soundness of the Portland cement*, and its setting time and stability were tested. Then, we added water and stirred well according to the water requirement of normal consistency. Next, we injected the mixture into the mold of 30 mm × 30 mm × 50 mm, and vibrated it. After 24 h, it was demoulded and put into a standard curing box with the temperature of (20 ± 1) °C and the humidity of more than 95%. The striding length ( $L_0$ ) was measured by ISO-160 comparator with an accuracy of 0.001 mm. Then, the standard curing was continued until the set age. After that, the length ( $l_1$ ) and its mechanical properties were determined. The central part of the test block was taken for phase composition and structure test.
- (3) Preparation and testing of GFPBM. The PSA and IOTs were mixed according to a certain cement sand ratio. Then we added some water, stirred the GFPBM, and then put it into the cement mortar triple testing mold (40 mm × 40 mm × 160 mm). And it vibrated on the cement mortar vibration platform. After 24 h, it was demoulded and put into a standard curing box with the temperature of (20 ± 1) °C and the humidity of more than 95%. Finally, the mechanical properties of the test block at different ages were determined.

## 2.3 Property characterization

The f-CaO content of SS was determined by EDTA complexometric titration according to Methods of Chemical Analysis of SS (YB/T 140-2009) with ethylene glycol as extractant. The f-MgO content was measured by using ammonium nitrate-ethanol as extractant. The SSA of materials was obtained with SSA-3200 (a dynamic specific surface area analyzer). The compressive strength test was conducted on the

samples based on the Chinese National Standard GB/T 17671-2021 *Method of testing cement-determination of strength*. The strength was measured by YES-300 (a hydraulic pressure testing machine) whose maximum load was 300 kN and the loading rate was 2.0 ± 0.5 kN/s. The value of mixture fluidity and slump were determined in accordance with GB/T 50,080–2016 *Standard for test method of performance on ordinary fresh concrete*.

The XRD spectra were obtained by a D/Max-RC diffractometer (Japan) with Cu-K $\alpha$  radiation whose working voltage was 40 kV and working current was 150 mA. Its 2  $\theta$  scanning ranged between 10° and 90°, and it could generate rays with the wavelength of 1.5406 nm. Through the Zeiss SUPRA™55 scanning electron microscope coupled with a Be4-U92 energy spectrum, SEM observation was performed to analyse the mineral phase and the hydration products of the paste samples.

SPLP is a method to evaluate the impact of BFPBM metal-leaching behavior. In this test, sulfuric acid or salpeter solution with the mass fraction of 60%/40% was added to adjust the pH to 4.20 ± 0.05, thus obtaining the leach liquor (Li and Chi, 2017). Then, the solidified powder of BFPBM with the particle size as 0.075 mm was mixed with the leach liquor according to the ratio of 1:20 (100 g of BFPBM solids/2,000 g leach liquor) and vibrated on a rotary agitator for 18 h. After that, the BFPBM slurry was filtered through a 0.45  $\mu$ m filter, and the concentrations of Cr, Ni, Cu, Cd, Pb, Zn, As, and Hg were determined via the inductively coupled plasma optical emission spectrometer (ICP-OES) (Zhu et al., 2017).

## 3 Results and discussion

### 3.1 Effect of SS fineness on the mechanical properties of BFPBM

SS was ground for 15, 30, 45, 60, and 75 min, and the obtained specific surface areas (SSA) were 252 m<sup>2</sup> kg<sup>-1</sup>, 386 m<sup>2</sup> kg<sup>-1</sup>, 457 m<sup>2</sup> kg<sup>-1</sup>, 487 m<sup>2</sup> kg<sup>-1</sup>, and 506 m<sup>2</sup> kg<sup>-1</sup>, respectively (see Figure 3). With the increase in grinding time, the SSA of SS presents an overall trend of

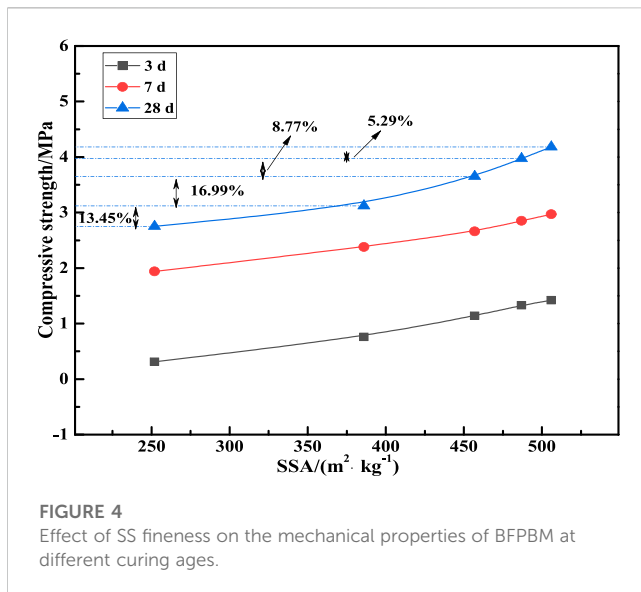


**FIGURE 4**  
Effect of SS fineness on the mechanical properties of BFPBM at different curing ages.

increasing. In particular, the SSA of SS increases rapidly when the grinding time is less than 45 min. When the grinding time continues from 15 min to 30 min and 45 min, the SSA increases by 53.21% and 18.35%, respectively. Then, the increasing speed slows down, and the SSA of SS increases by 6.51% and 3.84% at 60 min and 75 min respectively. After 45 min grinding, the SSA of the SS is 457 m<sup>2</sup>·kg<sup>-1</sup>. After the preliminary exploration experiment, the mix proportion of optimized PSA was SS: FGDG: GBFS=50:12:38, and the SSAs of FGDG and GBFS after grinding were 390 m<sup>2</sup>·kg<sup>-1</sup> and 480 m<sup>2</sup>·kg<sup>-1</sup>, respectively. The mixing ratio of PSA was 1:5, and the paste mass concentration (PMC) was set as 70%. The influence of SS fineness on BFPBM under different grinding times was studied, as shown in Figure 4.

As can be seen from Figure 4, with the increase of the SSA of SS, the compressive strengths of BFPBM at 3 d, 7 d and 28 d all show an increasing trend. Similar to the conclusion of SSA in Figure 3, when the SSA of SS is within 457 m<sup>2</sup>·kg<sup>-1</sup>, the compressive strength of BFPBM at each curing age will grow rapidly. Later, as the SSA continues to increase, the strength grows slowly. Therefore, the 28 d compressive strength of BFPBM is taken as an example. As the SSA of SS is increased from 252 m<sup>2</sup>·kg<sup>-1</sup>–386 m<sup>2</sup>·kg<sup>-1</sup>, and then increased to 457 m<sup>2</sup>·kg<sup>-1</sup>. The compressive strength of BFPBM is increased by 13.45% and 16.99%, respectively. Subsequently, the increasing rate of the compressive strength of BFPBM slows down to 8.77% and 5.29%. Therefore, when the SSA of SS is 457 m<sup>2</sup>·kg<sup>-1</sup>, the BFPBM has the compressive strength of 1.14, 2.66 MPa and 3.65 MPa at 3 d, 7 d and 28 d, respectively. It can be seen that when the grinding time of SS is greater than 45 min, the SSA of SS and the compressive strength of BFPBM prepared is increased slowly. Considering the grinding efficiency and cost, the optimal grinding time of SS is 45 min, at which the SSA of SS is 457 m<sup>2</sup>·kg<sup>-1</sup> and BFPBM has high compressive strength.

### 3.2 Effect of SS content on the mechanical properties of BFPBM

Considering the soundness of SS, the mixing amount of SS was tested, and the mix proportion was shown in Table 2. The FGDG

content was 10%. The SSAs of FGDG and GBFS after grinding were 390 m<sup>2</sup>·kg<sup>-1</sup> and 480 m<sup>2</sup>·kg<sup>-1</sup>. The mixing ratio of PSA was 1:5, and the PMC was 79%. Then, the obtained sample was determined at the specified age (3 d, 7 d, and 28 d) to obtain the compressive strength. The experimental results are shown in Figure 5.

With the fixed mixing ratio of PSA and the content of FGDG, as the SS content decreases, the compressive strength of BFPBM in each age increases first and then decreases. When the SS content decreases from 68% to 58%, the 28d compressive strength is higher than the initial value (G1-28 d compressive strength) of 48.44%. With the further reduction of the SS content, the 28d compressive strength of BFPBM decreases, and the 28 d compressive strength of G7 decreases by 35.50% compared with that of G3. Compared with the 28d compressive strength of the BFPBM, the variation trends of the compressive strengths at 3 d and 7 d are the same as that of the 28 d compressive strength. When the SS content is 58%, the compressive strength of BFPBM is the maximum, and the experimental result of G3 is the best. That is, the PSA mix proportion is SS: GBFS: FGDG=58:32:10, the cement sand ratio is 1:5, and PMC is 79%. At this time, the 3 d, 7 d and 28 d compressive strengths of the BFPBM are 1.87 MPa, 3.26 MPa, 5.24 MPa, respectively. It meets the requirement of 0.4 MPa strength in Chinese National Standard T/CECS 1037–2022 *Technical Standard for backfilling project by using premixed fluid solidifying soil*.

### 3.3 Effect of WRA dosage on the properties of BFPBM

The water-reducing agent (WRA) is a kind of concrete admixture applied in the field of building materials. The mechanism of WRA contains: dispersion, lubrication, steric hindrance, and sustained release. WRA can reduce the mixing water consumption with the slump of concrete basically unchanged. It can be used to disperse the mixture, improve its working property, reduce unit water consumption, enhance the fluidity of the mixture, and reduce unit cementitious material consumption.

In this study, the material mix proportion determined in Section 3.2 was adopted. The PMC was 79%, and polycarboxylate superplasticizer (PC) was selected as the WRA. The dosages of PC accounted for 0.14%, 0.15%, 0.16%, 0.17%, 0.18%, 0.19%, and 0.20% of the weight of PSA, respectively. The corresponding experimental numbers were W1, W2, W3, W4, W5, W6, and W7. The effect of PC dosage on the property of BFPBM is shown in Figures 6, 7.

As can be seen from Figure 6, when the PMC is 79%, the slump of the BFPBM with PC is significantly higher than that without PC, which meets the slump requirement (150 mm < slump < 240 mm) in Chinese National Standard T/CECS 1037–2022 *Technical Standard for backfilling project by using premixed fluid solidifying soil*.

With the same PMC, the slump of BFPBM increases significantly after adding PC, which is higher than that without adding PC (175 mm). With the increase of PC content, the slump increases first and then decrease. When the content of PC is 0.18%, the maximum slump reaches 215 mm. The addition of PC is beneficial to improve the mechanical properties of the BFPBM system.

TABLE 2 Mix proportion of BFPBM.

Number	Composition of PSA/%			Cement sand ratio	PMC/%
	SS	FGDG	GBFS		
G1	68	10	22	1:5	79
G2	63	10	27	1:5	79
G3	58	10	32	1:5	79
G4	53	10	37	1:5	79
G5	48	10	42	1:5	79
G6	43	10	47	1:5	79
G7	38	10	52	1:5	79

Note: PMC, solid mass/(solid mass +liquid mass) ×100%.

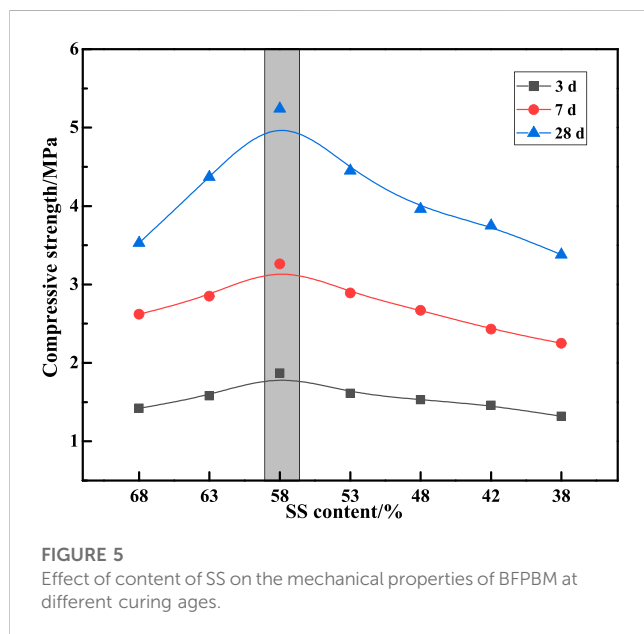


FIGURE 5 Effect of content of SS on the mechanical properties of BFPBM at different curing ages.

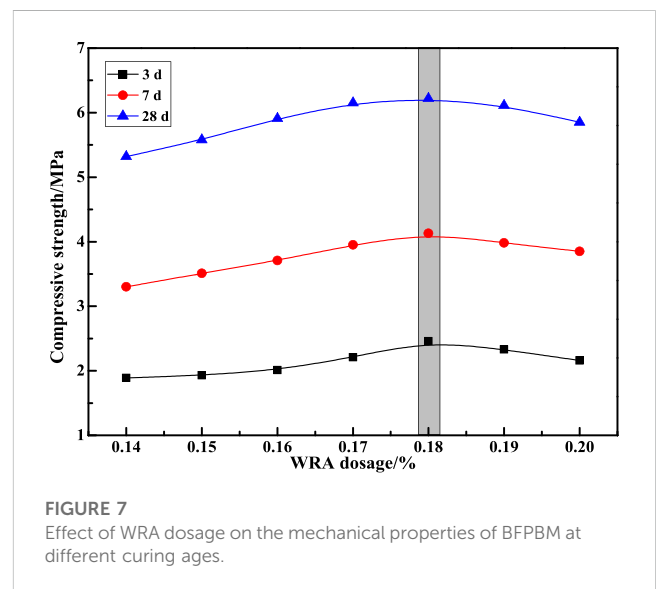


FIGURE 7 Effect of WRA dosage on the mechanical properties of BFPBM at different curing ages.

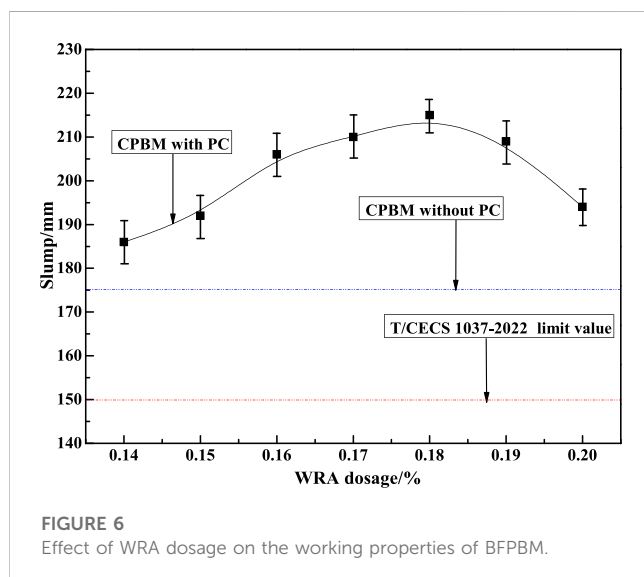


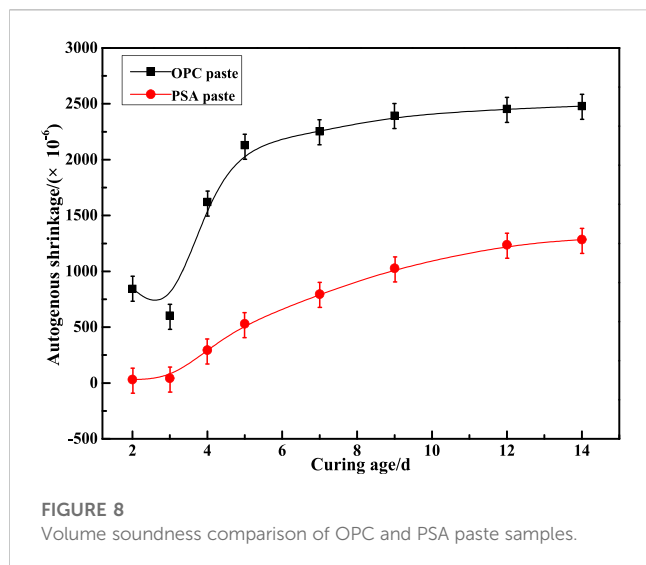
FIGURE 6 Effect of WRA dosage on the working properties of BFPBM.

Figure 7 shows the trend diagram of the mechanical properties of the BFPBM when the PMC is 79%. The bending strengths and compressive strengths of the BFPBM sample with PC at 3 d, 7 d, and 28 d are obviously better than those without PC in Figure 5. The compressive strengths of the BFPBM samples with 0.18% PC at 3 d, 7 d, and 28 d increased by 31.56%, 26.69% and 18.70%, respectively, compared with the samples without PC at the same age.

The compressive strengths of the BFPBM mixed with 0.18% PC reach 2.46 MPa, 4.13 MPa, and 6.22 MPa at 3 d, 7 d and 28 d, respectively. They all meet the strength index (>0.4 MPa) in Chinese National Standard T/CECS 1037-2022. Compared with most building foundation pit backfilling requirements, the strength of the BFPBM is relatively higher. In application, the water-binder ratio and slump can be selected and adjusted more reasonably according to the specific requirements of BFPBM for strength and pumping conditions.

### 3.4 Soundness analysis of BFPBM

From Section 3.3, the full solid waste PSA with the mix proportion of SS: GBFS: FGDG=58:32:10 was prepared into paste



according to the water-cement ratio of 1:2. Then, initial setting, final setting and fluidity tests were conducted, and no water seepage phenomenon was found in the PSA paste, proving its good water-retaining properties. The initial setting time of PSA was 162 min and the final setting time was 246 min, which could not only ensure the conveying and backfilling of BFPBM, but also facilitate solidification and improve the backfilling efficiency. The fluidity of the PSA paste was 136 mm, which also meets the fluidity requirement of the PSA for fertilizer tank backfilling (>100 mm) specified in Chinese National Standard T/CECS 1037-2022.

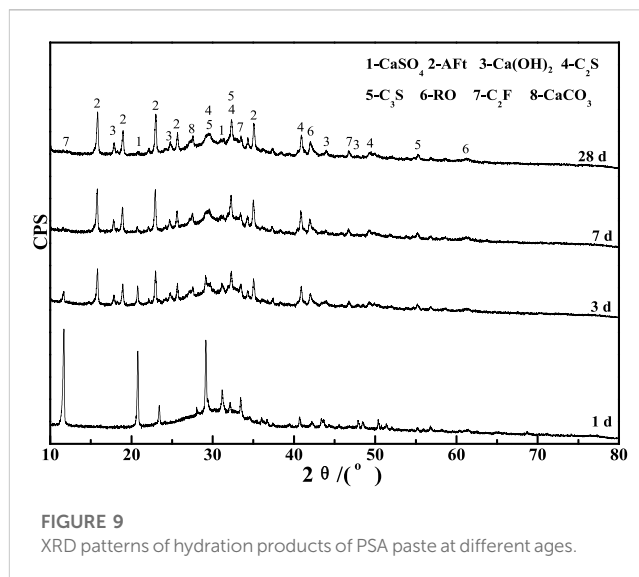
Since the BFPBM contains SS, it has soundness problems. It is necessary to test the volume soundness. In our test, the volume expansion values of two groups of samples were measured by the Le Chatelier Needles, and the results were 2.2 mm and 2.5 mm, respectively. This proved that the soundness was qualified. With OPC as the control group, we measured the changes in the volume soundness of the paste samples prepared by PSA at different ages, as shown in Figure 8.

It is reflected in Figure 8 that both paste samples present shrinkage characteristics under the standard condition, but their shrinkage degrees are obviously different: the shrinkage degree of the latter is smaller. At 14 d, the shrinkage values of the two samples were  $2480 \times 10^{-6}$  and  $1285 \times 10^{-6}$ , respectively. The shrinkage values of the PSA samples with SS at 14 d were 48.2% lower than that of OPC at the same age. The volume soundness of the newly prepared PSA was better than that of the ordinary Portland cement. In summary, it can be seen that the optimal proportion of PSA is determined through the test, and its working performance and soundness meet the standard requirements, making it suitable for the next practical engineering.

## 3.5 Hydration mechanism analysis of PSA

### 3.5.1 XRD analysis

The PSA paste sample with the water-binder ratio of 0.5 was prepared according to the optimized mix proportion. The hydration products of the paste sample were cured for 1 d, 3 d, 7 d and 28 d, as shown in Figure 9. As can be seen from their XRD patterns, the



following substances are observed, including ettringite (AFt),  $\text{Ca}(\text{OH})_2$ , RO phase,  $\text{CaSO}_4$ ,  $\text{C}_2\text{F}$ ,  $\text{CaCO}_3$ , and unhydrated  $\text{C}_3\text{S}$  and  $\text{C}_2\text{S}$ . SS is similar to cement clinker, in which active minerals  $\text{C}_3\text{S}$  and  $\text{C}_2\text{S}$  undergo hydration reaction to form C-S-H gel and  $\text{Ca}(\text{OH})_2$ . There is an obvious “bulge” at  $25\text{--}35^\circ$ , indicating that the system contains a large number of C-S-H gels and amorphous substances with low crystallinity (Bensted and Barnes, 2002; Wang et al., 2016; Wang et al., 2019). With the extension of the curing age, C-S-H gels are continuously deposited, gradually thickening and hardening the paste, and rapidly increasing its macroscopic strength (Cui et al., 2017). There is the amorphous vitreous body  $((\text{CaO})_m(\text{SiO}_2)_n(\text{Al}_2\text{O}_3)_k)$  in SS and GBFS, which can be illustrated by the steamed bread peaks between  $25^\circ \sim 35^\circ$  (Figures 1A, B). Since the vitreous body has volcanic activity (Mejdi et al., 2019), the  $\text{Ca}(\text{OH})_2$  generated by the hydration of  $\text{C}_3\text{S}$  and  $\text{C}_2\text{S}$  in SS will consume the glass phase of SS and GBFS. Therefore, the diffraction summit of  $\text{C}_3\text{S}$  and  $\text{C}_2\text{S}$  in Figure 9 will gradually weaken with the extension of curing time. AFt diffraction peaks appear at  $2\theta$  of  $15.7^\circ$ ,  $19.0^\circ$ ,  $23.1^\circ$  and  $32.3^\circ$ , and the AFt diffraction peaks gradually increase with the extension of curing age. Since the generation of AFt consumes  $\text{CaSO}_4$  in FGDG, the diffraction summit of  $\text{CaSO}_4$  in hydration products decreases with the extension of age (Li et al., 2017; Wu et al., 2019).

In our test, after curing 1-day paste sample, hydration products did not change greatly and mainly contained more  $\text{C}_3\text{S}$ ,  $\text{C}_2\text{S}$  and  $\text{CaSO}_4 \cdot 2\text{H}_2\text{O}$ . The contents of  $\text{Ca}(\text{OH})_2$  and AFt increased significantly with the curing age increasing to 3 d, which was because the  $\text{Ca}(\text{OH})_2$  generated by the hydration of  $\text{C}_3\text{S}$  and  $\text{C}_2\text{S}$  in SS created an alkaline environment for the system. Therefore, more  $\text{Ca}^{2+}$  and  $\text{Al}^{3+}$  ions were dissociated from the GBFS vitreous body to generate C-S-H gels, and they reacted with  $\text{SO}_4^{2-}$  provided by FGDG to form AFt (see Eq. 1), making the diffraction peaks of  $\text{C}_3\text{S}$ ,  $\text{C}_2\text{S}$  and  $\text{CaSO}_4 \cdot 2\text{H}_2\text{O}$  in Figure 9 drop significantly. The contents of  $\text{Ca}(\text{OH})_2$  and AFt in the system continued to increase when the curing age reached 7 d, and the reaction continued. When the age increased 28 d, the content of  $\text{CaSO}_4 \cdot 2\text{H}_2\text{O}$  in the system was basically exhausted, and the

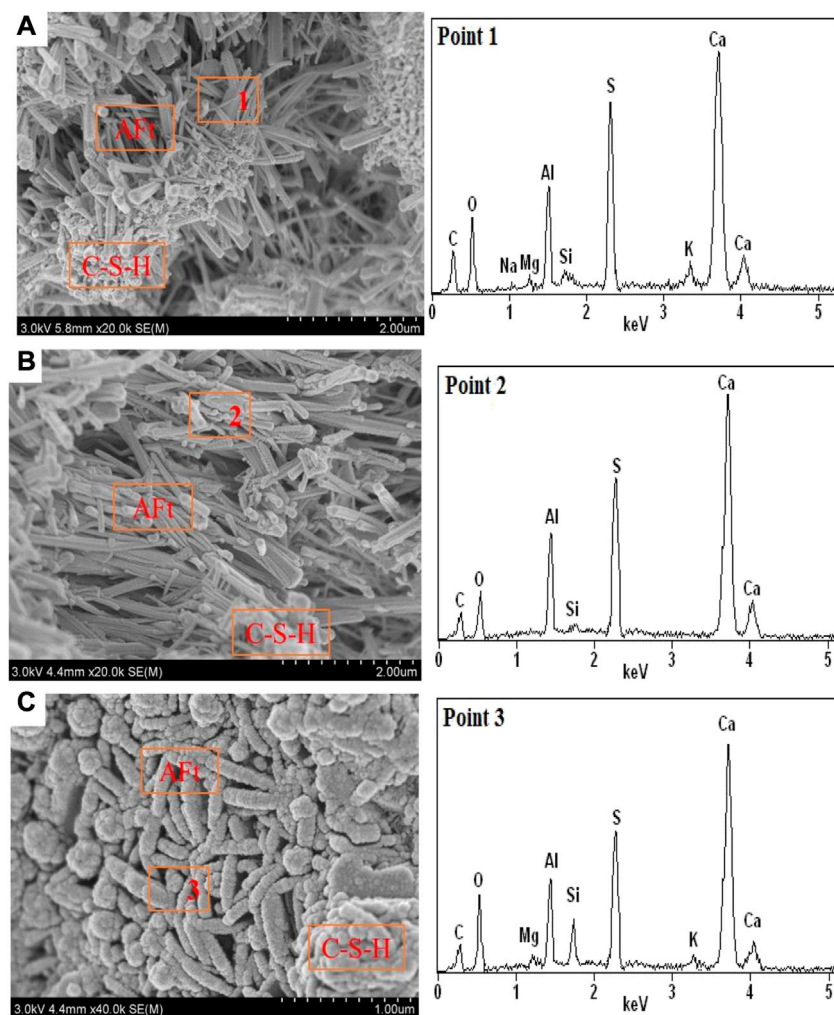
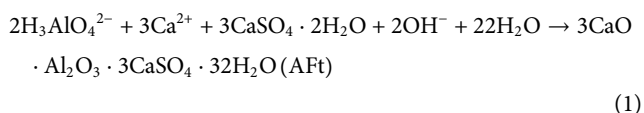


**FIGURE 10**  
SEM-EDS images of hydration products of PSA paste at different ages. (A) 3 d; (B) 7 d; (C) 28 d.

content of AFt tended to be stable. In addition, the RO phase in the system basically did not participate in the hydration reaction, and the hydration entered the stable stage.



The diffraction peak of  $\text{Ca}(\text{OH})_2$  was low in the early stage of hydration, which was related to its low crystallinity and partial absorption by GBFS hydration (Jiang et al., 2018). With the progress of hydration, the content of  $\text{Ca}(\text{OH})_2$  increased at 3 d of hydration, the content of  $\text{Ca}(\text{OH})_2$  basically remained unchanged at 28 d of hydration, and the hydration entered a stable stage. With SS, GBFS and FGDG stimulating each other, the system shows good hydraulic cementing characteristics, and the three synergistically promote the hydration reaction to continue.

Compared with Portland cement clinker, SS has fewer contents of CaO and  $\text{C}_3\text{S}$ , indicating that it can be regarded as a weak Portland cement clinker. Therefore, it needs to be fully excited.

FGDG is a sulfate activator, which can accelerate the crystal precipitation of hydration products and improve the material compactness (Duan et al., 2018). The soundness of SS is improved after mechanical grinding, and GBFS powder can absorb f-CaO and f-MgO of SS to a certain extent. In addition, the activity of GBFS is much higher than that of SS, which can improve the strength of cementing materials, making the advantages of the two materials complementary (Zhang et al., 2019).

### 3.5.2 SEM-EDS analysis

Figure 10 shows the SEM-EDS images of the dried hydration products of PSA paste samples which were cured to different ages and then immediately mixed with the anhydrous ethanol solution to end the hydration. As can be seen from Figure 10, the hydration products of PSA are mainly rod-shaped AFt crystals and amorphous C-S-H gels.

After 3 d of hydration, rod-shaped AFt crystals of about 10  $\mu\text{m}$  and a small number of amorphous C-S-H gels in tiny voids appeared (Figure 10A). However, the crystallization of AFt crystal was incomplete, and the content of C-S-H gels was small, which was



**TABLE 3** The leaching concentrations of heavy metals from some raw materials, the PSA paste block and the BFPBM block after 28d curing age ( $\mu\text{g/L}$ ).

Materials	Cu	Pb	Zn	Ni	Cd	Cr	As	Hg
SS	6.419	0.07	25.47	0.0175	0.3641	0.793	0.0047	—
GBFS	0.028	0.42	0.33	0.0009	0.0013	2.021	0.0056	—
FGDG	0.93	1.84	24.63	0.0049	0.2818	2.556	0.1873	0.06258
IOTs	19.33	0.85	63.31	0.8830	0.4231	0.879	2.5215	0.00224
PSA paste block	1.765	0.03	12.38	0.0438	0.1526	1.012	0.5762	0.01360
BFPBM block	8.246	0.18	40.62	0.0564	0.2473	1.605	0.8525	0.00356
Limiting value	100	5	100	5	1	5	5	0.1

not enough to obtain a dense surface of the structure. As a result, the strength was not greatly improved.

After 7 d of hydration, the number of C-S-H gels and AFt crystals increased (Figure 10B). This made the structure tend to be reticular and denser, further improving the strength.

After further hydration for 28 d, the EDS spectra of each site showed that the main elements were Ca, Si and Al, which was consistent with those of AFt (Figure 10C). At this curing age, SS, GBFS and FGDG stimulated each other to further promote hydration, and the obtained C-S-H gels and AFt were interwoven. Consequently, we obtained a tight network structure with closer arrangement of particles, further improving the strength of the test blocks. Thus, BFPBM could have good macro strength (Li et al., 2020).

### 3.6 Environmental impact of BFPBM

At present, one of the focuses of iron and steel solid waste application research is its application in the field of building materials, but little attention is attached to its heavy metal leaching problem. SS, GBFS, and FGDG, as the iron and steel waste and the corresponding building materials, contain Cr, Zn, Cu, Ni, Pb, Cd, As and other heavy metals (Zhang et al., 2018; Young et al., 2021; Sarathchandra et al., 2022). They are easy to transfer and transform in the environment, presenting potential environmental risks.

In this study, the leaching toxicity of BFPBM raw materials (SS, GBFS, FGDG, and IOTs), PSA paste blocks and BFPBM blocks were separately tested by the SPLP test. The SSA of SS powder milled for 45 min was  $457 \text{ m}^2 \text{ kg}^{-1}$ , that of GBFS was  $480 \text{ m}^2 \text{ kg}^{-1}$ , and that of FGDG was  $390 \text{ m}^2 \text{ kg}^{-1}$ . The chemical composition of IOTs raw materials is shown in Table 1, and the composition of grain size is shown in Figure 2. PSA mix proportion is SS: GBFS: FGDG=58:32:10. The water-binder ratio for preparing the PSA paste block is 0.5. The cement sand ratio for preparing the BFPBM block is 1:5, PMC is 79%, and the content of WRA is 0.18% of the mass of PSA.

The PSA paste block and the BFPBM block were cured for 28 d, then leaching toxicity was tested. The results of leaching toxicity are shown in Table 3. Although heavy metal leaching was detected in raw materials and samples under acidic environment, the content of heavy metals was still far lower than the standard value of leaching toxicity evaluation stipulated in Chinese National Standard GB/T 5085.3-2007. In addition, as the

formation of hydration products C-S-H gels and AFt in PSA and BFPBM contributed to hydration stabilization, the risk of heavy metal leaching was further reduced. Therefore, it can be expected that even if raw materials with heavy metal leaching are added to the BFPBM system, the environmental risk coefficient of its application is still lower than the limit value specified in Chinese National Standard GB/T 5085.3-2007.

## 4 Conclusion

This paper used steel slag (SS), granulated blast furnace slag (GBFS) and flue gas desulfurization gypsum (FGDG) after mechanical activation to prepare building foundation pit backfilling materials (BFPBM) with the coordination of iron ore tailings (IOTs). By studying the composition, performance, hydration mechanism and environmental impact of BFPBM, the following conclusions are drawn.

- (1) After mechanical activation, the steel waste (SS, GBFS and FGDG), can replace the cement to prepare the full solid waste PSA. The PSA can be used to prepare the BFPBM with the coordination of IOTs, which provides a new path to study the resource utilization of steel waste.
- (2) As the mix proportion of PSA is SS: GBFS: FGDG=58:32:10, PMC is 79%, PSA incorporation ratio is 20%, and the added PC (a water-reducing agent) accounts for 0.18% of PSA total, the slump of BFPBM is 215 mm, and 28 d compressive strength reaches 6.22 MPa. Both meet the requirements of T/CECS 1037-2022 *Technical Standard for filling of Ready-mixed fluidized solidified soil*. The fluidity of PSA paste is 136 mm, and the soundness is qualified and better than that of P-O 42.5 ordinary Portland cement.
- (3) In the BFPBM system, SS, GBFS and FGDG can stimulate each other and further promote hydration. PSA hydration products include  $\text{C}_3\text{S}$ ,  $\text{C}_2\text{S}$ ,  $\text{Ca}(\text{OH})_2$ , C-S-H gels, AFt, RO phase,  $\text{CaCO}_3$ , and  $\text{C}_2\text{F}$ . With the increase of curing time,  $\text{C}_3\text{S}$ ,  $\text{C}_2\text{S}$ , and  $\text{CaSO}_4$  gradually disappear, and the contents of AFt and C-S-H gels increase continuously.
- (4) According to the environmental risk evaluation, BFPBM has low leaching toxicity, lower than the limit stipulated by Chinese National Standard GB5085.3-2007. It proves that it has high strength and good environmental friendliness. Therefore, BFPBM

has a good application prospect in building foundation pit backfilling and mine filling.

Handan Science and Technology Research and Development Program (21422111260).

## Data availability statement

The original contributions presented in the study are included in the article/[Supplementary Material](#), further inquiries can be directed to the corresponding authors.

## Author contributions

HZ proposes method and writes manuscript; CW and YZho propose and participates in design research and reviews paper; QY, JJ, KZ, YZhe, YZha, and FL participate in design research and reviews paper. All the authors approved the final version of the manuscript.

## Funding

The authors gratefully acknowledge financial support by the National Key Research and Development Program of China (No. 2021YFC1910605), the Natural Science Foundation of Hebei Province (E2020402079), State Key Laboratory of Solid Waste Resource Utilization and Energy Conservation (SWR-2023-007), Science and Technology Research and Development Plan of China Railway Construction Group Co., Ltd. (No. 22-11b, 22-14b),

## Conflict of interest

Authors YZhe and FL were employed by China Railway Construction Group Co., Ltd. and Construction Development Co., Ltd.

The remaining authors declare that the research was conducted in the absence of any commercial or financial relationships that could be construed as a potential conflict of interest.

## Publisher's note

All claims expressed in this article are solely those of the authors and do not necessarily represent those of their affiliated organizations, or those of the publisher, the editors and the reviewers. Any product that may be evaluated in this article, or claim that may be made by its manufacturer, is not guaranteed or endorsed by the publisher.

## Supplementary material

The Supplementary Material for this article can be found online at: <https://www.frontiersin.org/articles/10.3389/feart.2023.1181974/full#supplementary-material>

## References

- Abdi, M. R., Ghalandarzadeh, A., and Shafiei, C. L. (2021). An investigation into the effects of lime on compressive and shear strength characteristics of fiber-reinforced clays. *J. Rock Mech. Geotech. Eng.* 13 (4), 885–898. doi:10.1016/j.jrmge.2020.11.008
- Alanyali, H., Cöl, M., Yilmaz, M., and Karagöz, Ş. (2009). Concrete produced by steel-making slag (basic oxygen furnace) addition in Portland cement. *Int. J. Appl. Ceram. Tec.* 6 (6), 736–748. doi:10.1111/j.1744-7402.2008.02317.x
- Aldeky, H., and Hattamleh, O. A. (2017). Experimental study on the utilization of fine steel slag on stabilizing high plastic subgrade soil. *Adv. Civ. Eng.* 2017, 9230279. doi:10.1155/2017/9230279
- Bensted, J., and Barnes, P. (2002). *Structure and performance of cements*. second ed. New York: Spon Press.
- Cui, X., Ni, W., and Ren, C. (2017). Hydration mechanism of all solid waste cementitious materials based on steel slag and blast furnace slag. *Chin. J. Mat. Res.* 31 (9), 687–694. doi:10.11901/1005.3093.2016.741
- Deng, Y., Zhao, Y., Liu, J., Gu, X., Cha, F., and Zhu, C. (2018). Na<sub>2</sub>SiO<sub>4</sub>-and cement-based activation on steel slag and its application in soft-soil stabilization. *China J. Highw. Transp.* 31 (11), 11–20. (in Chinese).
- Dhoble, Y., and Ahmed, S. (2018). Review on the innovative uses of steel slag for waste minimization. *J. Mat. Cycles Waste Manag.* 20, 1373–1382. doi:10.1007/s10163-018-0711-z
- Duan, S., Liao, H., Cheng, F., Song, H., and Yang, H. (2018). Investigation into the synergistic effects in hydrated gelling systems containing fly ash, desulfurization gypsum and steel slag. *Constr. Build. Mat.* 187, 1113–1120. doi:10.1016/j.conbuildmat.2018.07.241
- Gencel, O., Karadag, O., Oren, O. H., and Bilir, T. (2021). Steel slag and its applications in cement and concrete technology: A review. *Constr. Build. Mat.* 283, 122783. doi:10.1016/j.conbuildmat.2021.122783
- Gu, X., Yu, B., Dong, Q., and Deng, Y. (2018). Application of secondary steel slag in subgrade: Performance evaluation and enhancement. *J. Clean. Prod.* 181, 102–108. doi:10.1016/j.jclepro.2018.01.172
- Guo, J., Bao, Y., and Wang, M. (2018). Steel slag in China: Treatment, recycling, and management. *Waste Manage* 78, 318–330. doi:10.1016/j.wasman.2018.04.045
- Hasita, S., Rachan, R., Suddeepong, A., Horpibulsuk, S., Arulrajah, A., Mohammadinia, A., et al. (2020). Performance improvement of asphalt concretes using steel slag as a replacement material. *J. Mat. Civ. Eng.* 32 (8), 04020227. doi:10.1061/(asce)mt.1943-5533.0003306
- Hasita, S., Suddeepong, A., Horpibulsuk, S., Samingthong, W., Arulrajah, A., and Chinkulkijniwat, A. (2020). Properties of asphalt concrete using aggregates composed of limestone and steel slag blends. *J. Mat. Civ. Eng.* 32 (7), 06020007. doi:10.1061/(asce)mt.1943-5533.0003148
- Huang, M., Sun, T., and Wang, L. (2020). Application of premixed solidified soil in backfilling of foundation trench. *IOP Conf. Ser. EES.* 510 (5), 052062. doi:10.1088/1755-1315/510/5/052062
- Humbert, P. S., and Castro-Gomes, J. (2019). CO<sub>2</sub> activated steel slag-based materials: A review. *J. Clean. Prod.* 208, 448–457. doi:10.1016/j.jclepro.2018.10.058
- Jiang, L., Li, C., Wang, C., Xu, N., and Chu, H. (2018). Utilization of flue gas desulfurization gypsum as an activation agent for high-volume slag concrete. *J. Clean. Prod.* 205, 589–598. doi:10.1016/j.jclepro.2018.09.145
- Jiao, W., Sha, A., Liu, Z., Li, W., Jiang, W., Qin, W., et al. (2020). Study on thermal properties of steel slag asphalt concrete for snow-melting pavement. *J. Clean. Prod.* 277, 123574. doi:10.1016/j.jclepro.2020.123574
- Li, J., and Chi, S. (2017). Innovative solidification/stabilization of lead contaminated soil using incineration sewage sludge ash. *Chemosphere* 173, 143–152. doi:10.1016/j.chemosphere.2017.01.065
- Li, J., Yu, Q., Wei, J., and Zhang, T. (2011). Structural characteristics and hydration kinetics of modified steel slag. *Cem. Concr. Compos.* 41 (3), 324–329. doi:10.1016/j.cemconres.2010.11.018
- Li, N., Farzadnia, N., and Shi, C. (2017). Microstructural changes in alkali-activated slag mortars induced by accelerated carbonation. *Cem. Concr. Res.* 100, 214–226. doi:10.1016/j.cemconres.2017.07.008
- Li, X., Li, K., Sun, Q., Liu, L., Yang, J., and Xue, H. (2021). Preparation of cemented oil shale residue–steel slag–ground granulated blast furnace slag backfill and its environmental impact. *Mater* 14 (8), 2052–2073. doi:10.3390/ma14082052
- Li, Y., Qiao, C., and Ni, W. (2020). Green concrete with ground granulated blast-furnace slag activated by desulfurization gypsum and electric arc furnace reducing slag. *J. Clean. Prod.* 269, 122212. doi:10.1016/j.jclepro.2020.122212

- Liu, J., Yu, B., and Wang, Q. (2020). Application of steel slag in cement treated aggregate base course. *J. Clean. Prod.* 269, 121733. doi:10.1016/j.jclepro.2020.121733
- Liu, W., Li, H., Zhu, H., and Xu, P. (2020). The interfacial adhesion performance and mechanism of a modified asphalt-steel slag aggregate. *Mater* 13 (5), 1180–1192. doi:10.3390/ma13051180
- Mason, B. (1944). The constitution of some open-heart slag. *J. Iron Steel Res. Int.* 179 (11), 69–80.
- Mejdi, M., Wilson, W., Saillio, M., Chaussadent, T., Divet, L., and Tagnit-Hamou, A. (2019). Investigating the pozzolanic reaction of post-consumption glass powder and the role of portlandite in the formation of sodium-rich C-S-H. *Cem. Concr. Res.* 123, 105790. doi:10.1016/j.cemconres.2019.105790
- Mo, L., Zhang, F., Deng, M., Jin, F., Al-Tabbaa, A., and Wang, A. (2017). Accelerated carbonation and performance of concrete made with steel slag as binding materials and aggregates. *Cem. Concr. Compos.* 83, 138–145. doi:10.1016/j.cemconcomp.2017.07.018
- Ning, J., and Huang, X. (2006). Experiment on structural formation and mechanism of strength increasing of stabilized soil. *J. B. Univ. Aeronaut. Astronaut.* 32 (01), 97–102. doi:10.1016/s1005-8885(07)60042-9
- Palankar, N., Shankar, A. U. R., and Mithun, B. M. (2016). Durability studies on eco-friendly concrete mixes incorporating steel slag as coarse aggregates. *J. Clean. Prod.* 129, 437–448. doi:10.1016/j.jclepro.2016.04.033
- Peng, Y., and Huang, C. (2010). Carbon steel slag as cementitious material for self-consolidating concrete. *J. Zhejiang Univ-SC. A* 11 (7), 488–494. doi:10.1631/jzus.A0900635
- Roslan, N., Ismail, M., Abdul-Majid, Z., Ghoreishiamiri, S., and Muhammad, B. (2016). Performance of steel slag and steel sludge in concrete. *Constr. Build. Mat.* 104, 16–24. doi:10.1016/j.conbuildmat.2015.12.008
- Sarathchandra, S. S., Rengel, Z., and Solaiman, Z. M. (2022). Remediation of heavy metal-contaminated iron ore tailings by applying compost and growing perennial ryegrass (*Lolium perenne* L.). *Chemosphere* 288, 132573. doi:10.1016/j.chemosphere.2021.132573
- Shen, J., Xu, Y., and You, G. (2018). Stabilized effect of desulfurized gypsum and steel slag blended clinker free cement on soft clay. *Bull. Am. Ceram. Soc.* 37 (12), 3888–3891. doi:10.16552/j.cnki.issn1001-1625.2018.12.029
- Shi, C. J. (2002). Characteristics and cementitious properties of ladle slag fines from steel production. *Cem. Concr. Res.* 32 (3), 459–462. doi:10.1016/S0008-8846(01)00707-4
- Shi, C. (2004). Steel slag-its production, processing, characteristics and cementitious properties. *J. Mat. Civ. Eng.* 16 (3), 230–236. doi:10.1061/(asce)0899-1561(2004)16:3(230)
- Sun, H., Wang, W., and Ling, S. (2021). Mechanical properties and microstructure of solidified soil with low cement content. *J. Zhejiang Univ-SC. B* 55 (3), 530–538. doi:10.3785/j.issn.1008-973X.2021.03.013
- Sun, R., Fang, C., Gao, F., Ge, Z., Zhang, H., Lu, Q., et al. (2021). The participation of basolateral amygdala in the efficacy of acupuncture with deqi treating for functional dyspepsia. *China J. Highw. Transp.* 34 (10), 216–230. doi:10.1007/s11682-019-00249-7
- Turner, L. K., and Collins, F. G. (2013). Carbon dioxide equivalent (CO<sub>2</sub>-e) emissions: A comparison between geopolymers and OPC cement concrete. *Constr. Build. Mat.* 43, 125–130. doi:10.1016/j.conbuildmat.2013.01.023
- Wang, A., He, M., Mo, L., Liu, K., Li, Y., Zhou, Y., et al. (2019). Research progress of building materials prepared from the carbonized curing steel slag. *Mat. Rep.* 33 (17), 2939–2948. doi:10.11896/cldb.19040202
- Wang, C., Ni, W., Zhang, S., Wang, S., Gai, G., and Wang, W. (2016). Preparation and properties of autoclaved aerated concrete using coal gangue and iron ore tailings. *Constr. Build. Mat.* 104, 109–115. doi:10.1016/j.conbuildmat.2015.12.041
- Wang, C., Ren, Z., Huo, Z., Zheng, Y., Tian, X., Zhang, K., et al. (2021). Properties and hydration characteristics of mine cemented paste backfill material containing secondary smelting water-granulated nickel slag. *Alex. Eng. J.* 60 (6), 4961–4971. doi:10.1016/j.aej.2020.12.058
- Wang, S., Li, X., Ren, K., and Liu, C. (2020). Experimental research on steel slag stabilized soil and its application in subgrade engineering. *Geotech. Geol. Eng.* 38, 4603–4615. doi:10.1007/s10706-020-01313-6
- Wang, S., Wang, C., Wang, Q., Liu, Z., Qian, W., Jin, C., et al. (2018). Study on cementitious properties and hydration characteristics of steel slag. *Pol. J. Environ. Stud.* 27 (1), 357–364. doi:10.15244/pjoes/74133
- Wang, Z., and Wang, D. (2022). Performance of industrial residue-cement solidified soils in resisting sulfate erosion. *Chin. J. Geotech. Eng.* 44 (11), 2035–2042. doi:10.11779/CJGE202211009
- Wu, M., Zhang, Y., Jia, Y., Sha, W., Liu, G., Yang, Z., et al. (2019). Effects of sodium sulfate on the hydration and properties of lime-based low carbon cementitious materials. *J. Clean. Prod.* 220, 677–687. doi:10.1016/j.jclepro.2019.02.186
- Xu, C., Ni, W., Li, K., Zhang, S., Li, Y., and Xu, D. (2019). Hydration mechanism and orthogonal optimisation of mix proportion for steel slag-slag-based clinker-free prefabricated concrete. *Constr. Build. Mat.* 228, 117036. doi:10.1016/j.conbuildmat.2019.117036
- Yan, P., Mi, G., and Wang, Q. (2014). A comparison of early hydration properties of cement-steel slag binder and cement-limestone powder binder. *J. Therm. Anal. Calorim.* 115 (1), 193–200. doi:10.1007/s10973-013-3360-4
- You, N., Shi, J., and Zhang, Y. (2020). Corrosion behaviour of low-carbon steel reinforcement in alkali-activated slag-steel slag and Portland cement-based mortars under simulated marine environment. *Corros. Sci.* 175, 108874. doi:10.1016/j.corsci.2020.108874
- Young, G., Chen, Y., and Yang, M. (2021). Concentrations, distribution, and risk assessment of heavy metals in the iron tailings of Yeshan National Mine Park in Nanjing, China. *Chemosphere* 271, 129546. doi:10.1016/j.chemosphere.2021.129546
- Yu, C., Cui, C., Wang, Y., Zhao, J., and Wu, Y. (2021). Strength performance and microstructural evolution of carbonated steel slag stabilized soils in the laboratory scale. *Eng. Geol.* 2021 (3), 106410. doi:10.1016/j.enggeo.2021.106410
- Yüksel, I. (2017). A review of steel slag usage in construction industry for sustainable development. *Environ. Dev. Sustain.* 19, 369–384. doi:10.1007/s10668-016-9759-x
- Zhang, G., Wu, P., Gao, S., Ye, P., Wang, C., Huo, Z., et al. (2019). Preparation of environmentally friendly low autogenous shrinkage whole-tailings cemented paste backfill material from steel slag. *Acta Microsc.* 28 (5), 961–971.
- Zhang, J., Li, S., and Li, Z. (2020). Investigation the synergistic effects in quaternary binder containing red mud, blast furnace slag, steel slag and flue gas desulfurization gypsum based on artificial neural networks. *J. Clean. Prod.* 273, 122972. doi:10.1016/j.jclepro.2020.122972
- Zhang, M., Li, K., Ni, W., Zhang, S., Liu, Z., Wang, K., et al. (2022). Preparation of mine backfilling from steel slag-based non-clinker combined with ultra-fine tailing. *Constr. Build. Mat.* 320, 126248. doi:10.1016/j.conbuildmat.2021.126248
- Zhang, X., Yang, H., and Cui, Z. (2018). Evaluation and analysis of soil migration and distribution characteristics of heavy metals in iron tailings. *J. Clean. Prod.* 172, 475–480. doi:10.1016/j.jclepro.2017.09.277
- Zhao, J., Wang, D., Yan, P., Zhang, D., and Wang, H. (2016). Self-cementitious property of steel slag powder blended with gypsum. *Constr. Build. Mat.* 113 (3), 835–842. doi:10.1016/j.conbuildmat.2016.03.102
- Zhao, Y., Wu, P., Qiu, J., Guo, Z., Tian, Y., Sun, X., et al. (2022). Recycling hazardous steel slag after thermal treatment to produce a binder for cemented paste backfill. *Power Technol.* 395, 652–662. doi:10.1016/j.powtec.2021.10.008
- Zhu, X., Chen, B., Zhu, L., and Xing, B. (2017). Effects and mechanisms of biochar-microbe interactions in soil improvement and pollution remediation: A review. *Environ. Pollut.* 227, 98–115. doi:10.1016/j.envpol.2017.04.032
- Zhuang, S., and Wang, Q. (2021). Inhibition mechanisms of steel slag on the early-age hydration of cement. *Cem. Concr. Res.* 140, 106283. doi:10.1016/j.cemconres.2020.106283